www.czasopisma.pan.pl PAN POLSKA AKADEMIA NAUK www.journals.pan.pl

Arch. Metall. Mater. **64** (2019), 4, 1239-1248

DOI: 10.24425/amm.2019.130086

J. MIETTINEN*, V-V. VISURI*, T. FABRITIUS*, N. MILCHEVA**, G. VASSILEV***#

THERMODYNAMIC DESCRIPTION OF TERNARY Fe-B-X SYSTEMS. PART 5: Fe-B-Si

Thermodynamic descriptions of the ternary Fe-B-Si system and its binary sub-system, B-Si, are developed in the context of a new Fe-B-X (X = Cr, Ni, Mn, V, Si, Ti, C) database. The thermodynamic parameters of the other binary sub-systems, Fe-Si and Fe-B, are taken from earlier assessments. Experimental thermodynamic and phase equilibrium data available in the literature has been used for the optimization of the thermodynamic parameters of the Fe-B-Si and B-Si systems. The solution phases are described using substitutional solution model and the compounds (silicides and borides) are treated as stoichiometric phases. The calculated and experimental thermodynamic and phase equilibrium data were found to be in good agreement.

Keywords: phase diagrams; thermodynamic modeling; Fe based systems; Fe-B-X systems thermodynamic database; Fe-B-Si system

1. Introduction

The current contribution builds upon our earlier started research [1] regarding the development of boron containing iron-based Fe-B-X database, where boron is treated as a substitutional component. To this end, a few pertinent descriptions have been published earlier [1-4].

A general Iron Alloys Database (IAD) is under development [5]. It contains simple-format thermodynamic data for solution phases and compounds comprising the following elements: Fe, Al, B, C, Ca, Ce, Cr, Cu, H, Mg, Mn, Mo, N, Nb, Ni, O, P, S, Si, Ti and V. The IAD is applied in the Inter Dendritic Solidification (IDS) solidification model [6-8], which can be used to simulate the non-equilibrium solidification of steels as well as their solid-state phase transformations, including precipitate formation or dissolution, depending on the cooling/heating history. As the IDS simulates non-equilibrium solidification. Simulation of non-equilibrium solidification inherently means that kinetics have been accounted for, i think this could be omitted, the calculation times are longer than in a conventional thermodynamic software simulating equilibrium solidification. However, calculation times can be decreased considerably by applying simple-format thermodynamic IAD-data. This is a clear benefit in real-time online processes of continuous casting, where one deals with numerous strand intersections needing simulation [9].

Although Si is not a transition metal like Cr, Ni or Mn, it is an important constituent of the steels and the Fe-B-Si system deserves an individual assessment. Experimental thermodynamic and phase equilibrium data available in the literature has been used for this purpose. Some relevant information has been presented by Tokunga et al. [10] and by Poletti and Battezzati [11]. However, it could not be used directly as their binary data are not compatible with the current database (where B is treated as substitutional constituent). In addition, the emphasis of the a.m. studies [10,11] is put on the glass formation phenomena, which is not considered in the present work.

The binary system descriptions are taken from [1] for Fe-B and from [12] for Fe-Si. The latter is a slightly modified version from previous Fe-Si optimizations [13, 14] ignoring the B2-ordering but including its effect to the stability of the disordered bcc phase. Hence, the data of [12] fits better for modelling of steels solidification and it has been retained for the current work.

The B-Si system was assessed by Zaitsev and Kodentsov [15]. Nevertheless, the combination of their interaction parameters with the unary SGTE data [16,17] lead to some unusual results. For example, beta-rhombo-B phase appeared stable in the middle of the B-Si phase diagram.

This system has also been assessed by Fries and Lukas [18], and by Tokunga et al. [19]. The former description [18], however, is rather complex for the current database, as it applies a three-sub-lattice model for the silicides. Neither was the latter description [19] suitable, because its Gibbs energy expression for pure Si, in beta-rhombo-B phase, is different from that of the current database and because the calculated liquid phase constituent activities do not agree so well with the measurements of [15]. Consequently, the B-Si system ought to be re-optimized in the current work.

* UNIVERSITY OF OULU, PROCESS METALLURGY RESEARCH UNIT, OULU, FINLAND
** MEDICAL UNIVERSITY OF PLOVDIV, FACULTY OF PHARMACY, PLOVDIV, BULGARIA
*** UNIVERSITY OF PLOVDIV, FACULTY OF CHEMISTRY, 24 TSAR ASEN STR.,4000 PLOVDIV, PLOVDIV, BULGARIA
# Corresponding author: gpvassilev@gmail.com

2. Theory (phases and their modeling)

Table 1 shows the phases and their modeling in the current Fe-B-Si assessment. The ternary solutions phases (liquid, bcc and fcc) are described with a substitutional solution model [20] while the binary and the ternary compounds (borides and silicides) are treated as stoichiometric phases.

TABLE 1

Phases and their modeling in the current Fe-B-Si description

Phase	Modeling
liquid (L)	(B,Fe,Si), substitutional, RKM[a]
bcc_A2 (bcc)	(B,Fe,Si), substitutional, RKM
fcc_A1 (fcc)	(B,Fe,Si), substitutional, RKM
dia_A4 (dia)	(B,Si), substitutional, RKM
beta-rhombo-B (bet)	(B,Si), substitutional, RKM
Fe_2Si	$(Fe)_2(Si)$, stoichiometric
Fe_5Si_3	$(Fe)_5(Si)_3$, stoichiometric
FeSi	(Fe)(Si), stoichiometric
$FeSi_2$-H	$(Fe)_3(Si)_7$, stoichiometric
$FeSi_2$-L	$(Fe)(Si)_2$, stoichiometric
Fe_2B	$(Fe)_2(B)$, stoichiometric
FeB	(Fe)(B), stoichiometric
SiB_n	$(Si)(B)_{15.67}$, stoichiometric
SiB_6	$(Si)(B)_6$, stoichiometric
SiB_3	$(Si)(B)_3$, stoichiometric
$Fe_{47}Si_{20}B_{10}$ (T_1)	$(Fe)_{47}(Si)_{20}(B)_{10}$, stoichiometric
$Fe_{50}Si_{10}B_{20}$ (T_2)	$(Fe)_{50}(Si)_{10}(B)_{20}$, stoichiometric
$Fe_{20}Si_4B_6$ (T_3)	$(Fe)_{20}(Si)_4(B)_6$, stoichiometric

[a] – Redlich-Kister-Muggianu (Gibbs excess energy model)

2.1. Solution phases

For a substitutional solution phase of the Fe-B-Si system, the molar Gibbs energy is expressed as

$$\begin{aligned} G_m^\phi = {} & x_{\mathrm{Fe}}^\phi \, {}^oG_{\mathrm{Fe}}^\phi + x_{\mathrm{B}}^\phi \, {}^oG_{\mathrm{B}}^\phi + x_{\mathrm{Si}}^\phi \, {}^oG_{\mathrm{Si}}^\phi + \\ & + RT(x_{\mathrm{Fe}}^\phi \ln x_{\mathrm{Fe}}^\phi + x_{\mathrm{B}}^\phi \ln x_{\mathrm{B}}^\phi + x_{\mathrm{Si}}^\phi \ln x_{\mathrm{Si}}^\phi) + \\ & + x_{\mathrm{Fe}}^\phi x_{\mathrm{B}}^\phi L_{\mathrm{Fe,B}}^\phi + x_{\mathrm{Fe}}^\phi x_{\mathrm{Si}}^\phi L_{\mathrm{Fe,Si}}^\phi + x_{\mathrm{B}}^\phi x_{\mathrm{Si}}^\phi L_{\mathrm{B,Si}}^\phi + \\ & + x_{\mathrm{Fe}}^\phi x_{\mathrm{B}}^\phi x_{\mathrm{Si}}^\phi L_{\mathrm{Fe,B,Si}}^\phi + {}^{mo}G_m^\phi \end{aligned} \tag{1}$$

where R is the gas constant (8.3145 J/K mol), T is the absolute temperature (K), x_i is the mole fraction of component i, ${}^oG_i^\phi$ is the molar Gibbs energy of pure component i in phase f expressed relative to the enthalpy of the component in its stable phase at 298.15 K [16, 20], $L_{i,j}^\phi$ is a binary parameter accounting for the interaction between components i and j in phase ϕ, and $L^\phi_{\mathrm{Fe,B,Si}}$ is a ternary interaction parameter of phase f. For these parameters, ${}^oG_i^\phi$ is a function of temperature, and $L_{i,j}^\phi$ and $L^\phi_{\mathrm{Fe,B,Si}}$ ($= L^\phi_{i,j,k}$) can be functions of temperature and composition. For the interaction parameters, the following composition dependencies [20-22] are possible

$$L_{ij}^\phi = \sum_{m=0}^{m_{\mathrm{MAX}}} {}^mL_{ij}^\phi (x_i^\phi - x_j^\phi)^m \tag{2}$$

$$L_{ijk}^\phi = v_i^\phi L_{iijk}^\phi + v_j^\phi L_{ijjk}^\phi + v_k^\phi L_{ijkk}^\phi \tag{3}$$

where m is the degree of the binary parameter (m_{MAX} = maximum degree) and v_i's are composition variables defined as $v_I = x_i + (1 - x_i - x_j - x_k)/3$. The advantage achieved by using the terms v_i as composition variables (instead of mole fractions), is that the sum of the v_i terms is always 1 in multicomponent systems [13,20]. In the present ternary Fe-B-Si description, Equation (3) is applied for the liquid phase whereas no ternary parameters are optimized for the bcc and fcc, phases, due to the very low solubility of boron in them.

The term ${}^{mo}G_m^\phi$ represents the contribution to the Gibbs energy due to the magnetic ordering expressed for solid solution phases, bcc and fcc, as suggested by Hillert and Jarl [23]

$${}^{mo}G_m^\phi = RT\ln(\beta^\phi + 1)\cdot f(\tau) \tag{4}$$

where β^ϕ is a composition-dependent parameter related to the total magnetic entropy and τ is defined as $\tau = T/Tc^\phi$ where Tc^ϕ is the critical temperature of magnetic ordering. The function $f(\tau)$ takes the polynomial form proposed by [23]. For the liquid phase, of course, ${}^{mo}G_m^\phi = 0$.

2.2. Compounds

All compounds of the binary Fe-B, Fe-Si and B-Si phase diagrams are treated as binary stoichiometric phases, as no solubility of a third component has been reported for them. The ternary compounds, $Fe_{47}Si_{20}B_{10}$, $Fe_{50}Si_{10}B_{20}$ and $Fe_{20}Si_4B_6$, are treated as stoichiometric phases, as suggested by Tokunga et al. [10], due to their negligible homogeneity ranges [24-26]. The binary and the ternary stoichiometric compounds Gibbs energies of formation are expressed as

$${}^oG_{A:B}^\phi = a\,{}^oG_A^\alpha + b\,{}^oG_B^\beta + A + BT \tag{5}$$

$${}^oG_{Fe,B,Si}^\phi = a\,{}^oG_{Fe}^{bcc} + b\,{}^oG_B^{bet} + c\,{}^oG_{Si}^{dia} + A + BT \tag{6}$$

where a, b and c are stoichiometric coefficients and ${}^oG_i^\theta$ is the molar Gibbs energy of pure component i in its stable phase at 298.15 K [16].

3. Experimental data

The experimental studies of the Fe-B-Si system have been reviewed by Raghavan [27]. Table 2 shows the experimental information selected for the current optimization of the B-Si and Fe-B-Si systems.

The phase equilibria of the B-Si system have been studied by several researchers [28-33] as reviewed by Olesinski and Abbaschian [34]. Some discrepancy appears in these measurements, in the vicinity of the eutectic reaction of L = dia + SiB_6, but otherwise, the agreement is reasonable. The thermodynamic properties of the liquid phase have been investigated by Zaitsev

TABLE 2

Experimental data applied for the optimization for the B-Si and Fe-B-Si systems

System	Experimental data	Reference
B-Si	Phase diagram	[15], [19], [28-33]
	Activity of B and Si in liquid alloys at 1577°C	[15]
Fe-B-Si	Liquidus projection and liquidus temperatures	[10], [35]
	Isothermal section at 900°C	[25]
	Three vertical sections at x_{Fe} = 0.8 & 0.65, x_B = 0.1 and x_{Si} = 0.1	[10], [11], [36]
	Enthalpy of mixing of liquid alloys at 1550°C	[37], [38]
	Gibbs energy of formation of liquid alloys at 1550°C	[37]
	Partial chemical potentials of B and Si in liquid alloys at 1500°C	[37]
	Partial chemical potential of Si in liquid alloys and 1350°C	[37]
	Partial chemical potential of B in liquid alloys at 1550 and 1455°C	[39]

and Kodentsov [15] using the Knudsen mass spectrometry. Boron and silicon activities in silicon-rich melts have been measured.

The Fe-Si-B system has been studied by several researchers. Poletti and Battezzati [11] used the differential scanning calorimetry to measure phase boundary transitions heat effects at cooling of iron-rich alloys, while Tokunga et al. [10] performed studies, both, at heating and at cooling. Nagumo and Sato [34] determined liquidus temperatures of iron-rich alloys from cooling curves. Some liquidus temperature determinations are also available from Desre [35].

Solid state phase equilibria have been studied by Aronsson and Engström [24], Chaban and Kuzma [25] and Efimov et al. [26]. Three near-stoichiometric compounds, $Fe_{47}Si_{20}B_{10}$, $Fe_{50}Si_{10}B_{20}$ and $Fe_{20}Si_4B_6$, were identified [24-26] and two isothermal sections were suggested, (at 1000°C [24] and 900°C [25]).

The thermodynamic properties of the liquid phase were investigated by Zaitsev et al. [37] using Knudsen-cell mass spectrometry and the integral variant of effusion method. Enthalpy of mixing of liquid alloys and liquid phase activities (i.e. chemical potentials) of boron and silicon were measured (Table 2). Measurements are available also from Witusievicz et al. [38], for liquid alloys enthalpy of mixing, and from Ball [39], for boron activities (chemical potentials) in iron-rich melts (Table 2).

4. Results and discussion

During the optimization process of both systems, B-Si and Fe-B-Si, priority was given to the liquid phase, for which experimental thermodynamic data are most available. Then, the Gibbs energy expressions of the compounds were adjusted with the experimental phase equilibrium data, first for SiB_n, SiB_6 and SiB_3 (B-Si system) and thereafter for $Fe_{47}Si_{20}B_{10}$, $Fe_{50}Si_{10}B_{20}$ and $Fe_{20}Si_4B_6$ (Fe-B-Si system). Gibbs energy expressions optimized in earlier studies have been used as start values. In spite of the emphasis given to the liquid phase, the whole optimization process was iterative, aiming at a reasonable evaluation of all parameters, at the same time.

The optimized Fe-B-Si system parameters are presented in Table 3. Those marked with a reference code are from earlier as-

TABLE 3

Thermodynamic description of the Fe-B-Si system. Thermodynamic data of pure components are taken from Dinsdale [16] unless shown otherwise in the table. Parameter values except for *Tc* and β are in J/mol. *Tc* and β are the Curie temperature (K) and the effective magnetic moment (magneton), of a phase, respectively

liquid (1 sublattice, sites: 1, constituents: B,Fe,Si)	Ref.
$L^L_{B,Fe} = (-133438 + 33.946T) + (+7771)(x_B - x_{Fe}) + (+29739)(x_B - x_{Fe})^2$	[40]
$L^L_{B,Si} = (+14000 - 8T) + (0)(x_B - x_{Si}) + (+14000 - 4T)(x_B - x_{Si})^2$	O*
$L^L_{Fe,Si} = (-164435 + 41.977T) + (-21.523T)(x_{Fe} - x_{Si}) + + (5220 + 5.726T)(x_{Fe} - x_{Si})^2 + (-28955 + 26.275T)(x_{Fe} - x_{Si})^3$	[12,14]
$L^L_{B,Fe,Si} = (0)x_B + (-40000 - 50T)x_{Fe} + (+150000 - 25T)x_{Si}$	O*
bcc (1 sublattice, sites: 1, constituents: B,Fe,Si)	
${}^oG^{bcc}_B = {}^oG^{bet}_B + (+43514 - 12.217T)$	[17]
$L^{bcc}_{B,Fe} = (-50000 + 42T)$	[1]
$L^{bcc}_{Fe,Si} = (-211000 + 80.2T) + (37000 - 74.5T)(x_{Fe} - x_{Si}) + (-10000 + 41.2T)(x_{Fe} - x_{Si})^2$	[12]
$Tc^{bcc} = 1043x_{Fe} + x_{Fe}x_{Si}(504(x_{Fe} - x_{Si}))$	[14]
$\beta^{bcc} = 2.22x_{Fe}$	[16]
fcc (1 sublattice, sites: 1, constituents: B,Fe,Si)	
${}^oG^{bcc}_B = {}^oG^{bet}_B + (+43514 - 12.217T)$	[17]
$L^{fcc}_{B,Fe} = (-66000 + 50T)$	[1]
$L^{fcc}_{Fe,Si} = (-125248 + 41.166T) + (-142708)(x_{Fe} - x_{Si}) + (89907)(x_{Fe} - x_{Si})^2$	[12-14]
$Tc^{fcc} = -201x_{Fe}$	[16]
$\beta^{fcc} = -2.1x_{Fe}$	[16]

dia (1 sublattice, sites: 1, constituents: B,Si) ${}^{o}G^{dia}{}_{B} = {}^{o}G^{bet}{}_{B} + (+20)$ $L^{dia}{}_{B,Si} = (+77500 - 25T)$	[17] O*
bet (1 sublattice, sites: 1, constituents: B,Si) ${}^{o}G^{bet}{}_{Si} = {}^{o}G^{dia}{}_{Si} + (+78625 - 68.25T + 0.015T^{2})$	O*
Fe_2Si (2 sublattices, sites: 2:1, constituents: Fe:Si) ${}^{o}G^{Fe2Si}{}_{Fe:Si} = 2{}^{o}G^{bcc}{}_{Fe} + {}^{o}G^{dia}{}_{Si} + (-71256.6 - 10.62T)$	[12-14]
Fe_5Si_3 (2 sublattices, sites: 5:3, constituents: Fe:Si) ${}^{o}G^{Fe5Si3}{}_{Fe:Si} = 5{}^{o}G^{bcc}{}_{Fe} + 3{}^{o}G^{dia}{}_{Si} + (-241144 + 2.16T)$	[12-14]
FeSi (2 sublattices, sites: 1:1, constituents: Fe:Si) ${}^{o}G^{FeSi}{}_{Fe:Si} = {}^{o}G^{bcc}{}_{Fe} + {}^{o}G^{dia}{}_{Si} + (-72761.2 + 4.44T)$	[12-14]
FeSi (2 sublattices, sites: 1:1, constituents: Fe:Si) ${}^{o}G^{FeSi}{}_{Fe:Si} = {}^{o}G^{bcc}{}_{Fe} + {}^{o}G^{dia}{}_{Si} + (-72761.2 + 4.44T)$	[12-14]
$FeSi_2$-H (2 sublattices, sites: 3:7, constituents: Fe:Si) ${}^{o}G^{FeSi2\text{-}H}{}_{Fe:Si} = 3{}^{o}G^{bcc}{}_{Fe} + 7{}^{o}G^{dia}{}_{Si} + (-196490 - 9.2T)$	[12-14]
$FeSi_2$-L (2 sublattices, sites: 1:2, constituents: Fe:Si) ${}^{o}G^{FeSi2\text{-}L}{}_{Fe:Si} = {}^{o}G^{bcc}{}_{Fe} + 2{}^{o}G^{dia}{}_{Si} + (-82149 + 10.44T)$	[12-14]
Fe_2B (2 sublattices, sites: 0.6667:0.3333, constituents: Fe:B) ${}^{o}G^{Fe2B}{}_{Fe:B} = 0.6667{}^{o}G^{bcc}{}_{Fe} + 0.3333{}^{o}G^{bet}{}_{B} + (-26261 + 3.466T)$	[40]
FeB (2 sublattices, sites: 0.5:0.5, constituents: Fe:B) ${}^{o}G^{FeB}{}_{Fe:B} = 0.5{}^{o}G^{bcc}{}_{Fe} + 0.5{}^{o}G^{bet}{}_{B} + (-35150 + 6T)$	[1]
SiB_n (2 sublattices, sites: 1:15.67 constituents: Si:B) ${}^{o}G^{SiBn}{}_{Si:B} = {}^{o}G^{dia}{}_{Si} + 15.67{}^{o}G^{bet}{}_{B} + (-207600 + 58T)$	O*
SiB_6 (2 sublattices, sites: 1:6, constituents: Si:B) ${}^{o}G^{SiB6}{}_{Si:B} = {}^{o}G^{dia}{}_{Si} + 6{}^{o}G^{bet}{}_{B} + (-154100 + 48T)$	O*
SiB_3 (2 sublattices, sites: 1:3 constituents: Si:B) ${}^{o}G^{SiB3}{}_{Si:B} = {}^{o}G^{dia}{}_{Si} + 3{}^{o}G^{bet}{}_{B} + (-117300 + 50T)$	O*
$Fe_{47}Si_{20}B_{10}$ (T_1) (3 sublattices, sites: 47:20:10, constituents: Fe:Si:B) ${}^{o}G^{T1}{}_{Fe:Si:B} = 47{}^{o}G^{bcc}{}_{Fe} + 20{}^{o}G^{dia}{}_{Si} + 10{}^{o}G^{bet}{}_{B} + (-2380000 + 50T)$	O*
$Fe_{50}Si_{10}B_{20}$ (T_2) (3 sublattices, sites: 50:10:20, constituents: Fe:Si:B) ${}^{o}G^{T2}{}_{Fe:Si:B} = 50{}^{o}G^{bcc}{}_{Fe} + 10{}^{o}G^{dia}{}_{Si} + 20{}^{o}G^{bet}{}_{B} + (-2457000 + 230T)$	O*
$Fe_{20}Si_4B_6$ (T_3) (3 sublattices, sites: 20:4:6, constituents: Fe:Si:B) ${}^{o}G^{T3}{}_{Fe:Si:B} = 20{}^{o}G^{bcc}{}_{Fe} + 4{}^{o}G^{dia}{}_{Si} + 6{}^{o}G^{bet}{}_{B} + (-864000 + 72T)$	O*

O* – Parameter optimized in this work.

sessments, and those marked with O* are optimized in the current study using the literature experimental data shown in Table 2.

The descriptions of the Fe-B and Fe-Si systems have been done by us previously [1,12].

For the binary B-Si and the ternary Fe-B-Si systems, the results calculated in this work are compared with the original experimental data to verify the optimization asshown in the following subsections. All calculations are carried out with the ThermoCalc software [41].

4.1. System B-Si

Calculated and experimental invariant points of the B-Si system are compared in Table 4. One can see that the agreement is reasonably good.

Figure 1 exhibits B-Si phase diagram calculated with the parameters obtained in this work, together with experimental data points [15,19,28-33]. The diagram calculated by Tokunga et al. [19] is shown by dotted curves. Si solubility in the bet phase at low temperatures is feebler in comparison with the measure-

TABLE 4

Calculated and experimental invariant points of the B-Si system

$\phi1 - \phi2 - \phi3$	Temp (°C)	$x_B^{\phi1}$	$x_B^{\phi2}$	$x_B^{\phi3}$	Ref.
L + beta	2020	0.907	0.970	0.959	Exp [33]
$= SiB_n$	2020	0.906	0.969	0.940	Cal This study
	2030	0.929	0.975	0.959	Cal [19]
	2020	0.907	0.970	0.940	Cal [15]
	2020	0.926	0.979	0.967	Cal [18]
$L + SiB_n$	1850	0.653	0.940	0.857	Exp [33]
$= SiB_6$	1850	0.627	0.940	0.857	Cal This study
	1857	0.649	0.959	0.857	Cal [19]
	1850	0.645	0.940	0.857	Cal [15]
	1850	0.621	0.941	0.862	Cal [18]
$L = dia + SiB_6$	1385	0.080	0.030	0.857	Exp [34]
	1381	0.123	0.035	0.857	Cal This study
	1394	0.098	0.020	0.857	Cal [19]
	1362	0.140	0.035	0.857	Cal [15]
	1384	0.081	0.011	0.854	Cal [18]
$dia + SiB_6$	1270	0.010	0.857	0.750	Exp [34]
$= SiB_3$	1270	0.019	0.857	0.750	Cal This study
	1272	0.013	0.857	0.750	Cal [19]
	1270	0.007	0.855	0.738	Cal [18]

ments of Armas et al. [32]. It was not possible to ameliorate the agreement without making the bet phase stable in the middle of the diagram. The situation is different when applying a sublattice model for that phase [18]. Note also the presence of the SiB_3 phase considered by Fries and Lukas [18] and Olesinski and Abbaschian [34] but not by Zaitsev and Kodentsov [15].

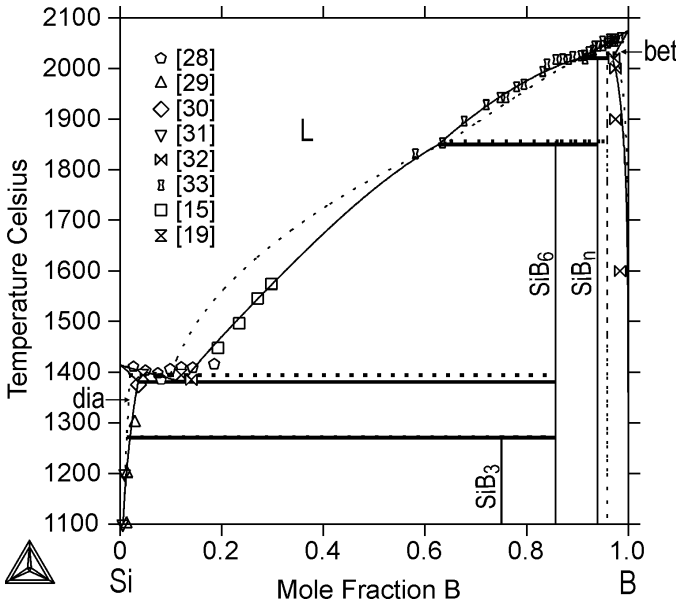

Fig. 1. B-Si phase diagram calculated with the parameters obtained in this work, together with experimental data points [15,19,28-33]. The diagram calculated by Tokunga et al. [19] is shown by dotted curves

Calculated activities of Si and B in liquid B-Si alloys at 1577°C (Figure 2), agree well with experimental data points of Zaitsev and Kodentsov [15]. The solid curves refer to the calculations of this study and dotted curves refer to those of Tokunga et al. [19].

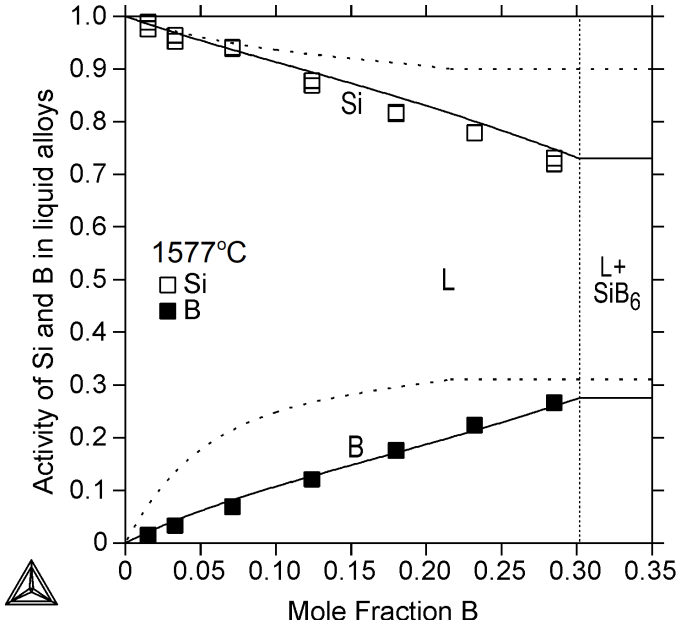

Fig. 2. Calculated activities of Si and B in B-Si alloys at 1577°C, together with experimental data points of Zaitsev and Kodentsov [15]. The solid curves refer to the calculations of this study and dotted curves refer to those of Tokunga et al. [19]. The reference states used are pure liquid Si and B

The present calculations agree with the experimental data of Zaitsev and Kodentsov [15] better than with these of Tokungaet al. [19]. Additional experimental data for boron activity coefficient in liquid alloys is available from [42-44]. These activity data show a large positive deviation from Raoult's law with $\gamma_B > 3.6$ and do not agree with the present calculations nor with the measurements of [15] giving $\gamma_B \approx 1$.

4.2. System Fe-B-Si

Figures 3-16 present the results obtained by the current optimization of the Fe-B-Si system, which agree reasonably well with the experimental data (Table 2). The calculated liquidus projection (Figure 3) should be considered as tentative, due to the lack of systematic experimental data for the different liquidus surfaces. The calculated monovariant lines of Desre et al. [35] concur well with the current calculationsat low Si contents, but these lines were not drawn to higher Si contents, as no ternary phases (T_1, T_2, T_3) were considered in their study.

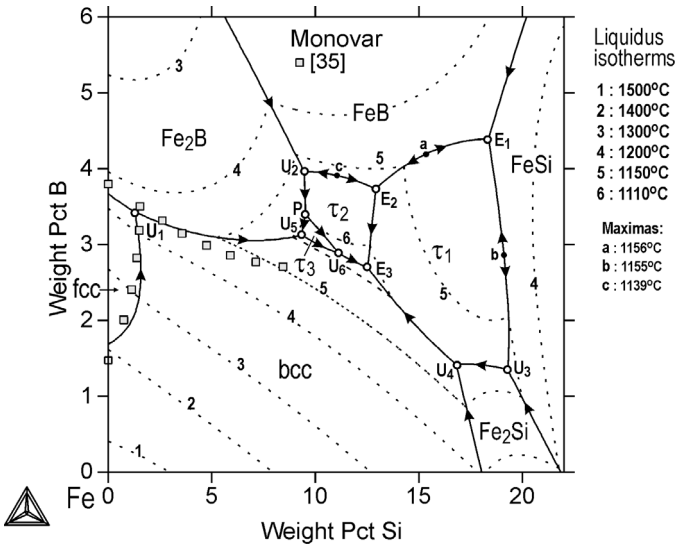

Fig. 3. Calculated primary surfaces of the Fe-B-Si system, together with the data points from the calculations of Desre et al. [35]. The calculated liquidus isotherms between 1500 and 1100°C (dotted curves) are plotted too

Figures 4 and 5 show two calculated isothermal sections of the system, at 1225 and 900°C, which agree reasonably well with the experimental data. It is important to note (Figure 4) the isolation (i.e. gradual disappearance) of the liquid phase as the temperature decreases below 1175°C.

Figures 6-9 show four calculated vertical sections of the system at $x_{Fe} = 0.80$, $x_{Fe} = 0.65$, $x_B = 0.1$ and $x_{Si} = 0.1$, where x_i is the mole fraction of the respective element. The agreement with the experimental data is reasonable. In Figure 6, the dotted lines show the liquidus surfaces and the eutectic temperature

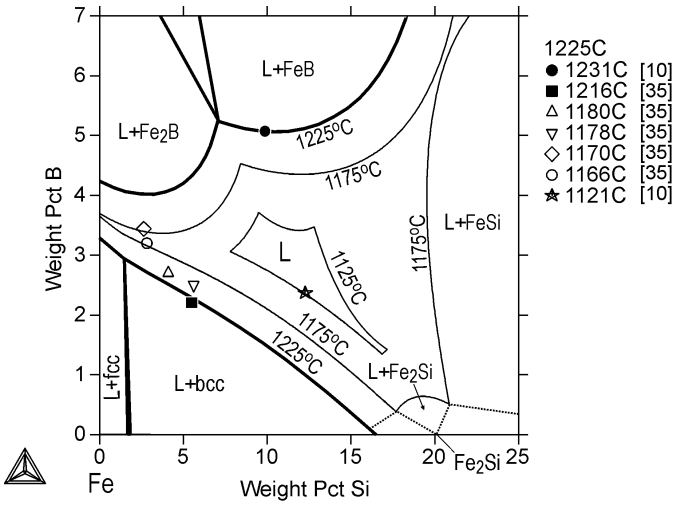

Fig. 4. Calculated isotherm of 1225°C (thick lines) and liquid regions of 1175 and 1125°C (thin lines) in the Fe-B-Si system, together with experimental data points of Tokunga et al. [10], and Desre et al. [35]

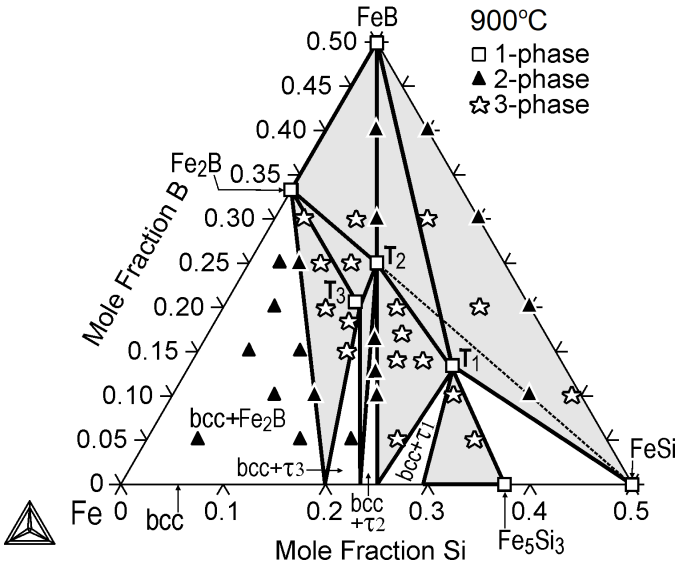

Fig. 5. Calculated isotherm of 900°C in the Fe-B-Si system, together with experimental data points of Chaban and Kuzma [25]. The broken line shows the FeSi-T_2 equilibrium suggested by [25]

calculated by Poletti and Battezzatti [11] and in Figures 7-9, they show the liquidus surfaces calculated by Tokunga et al. [10].

It is of worth noting that the correlation between the calculated liquidus lines and the measured data points in the silicon-poor regions of Figures 6 through 8 and the boron-poor region of Figure 9 is moderate. This discrepancy could not be reduced by modifying the binary Fe-B and Fe-Si descriptions, because they well agree with the corresponding binary measurements [1,12]. Another reason to keep these binary descriptions untouched is that they have already been used in other ternary optimizations of the IAD database. Indeed, it is more likely, that most of the mentioned discrepancies are due to the measurements themselves. For example, Tokunga et al. [10] stated that the measurements of Nagumo and Sato [36] may have been affected by supercooling, due to the high amorphization ability of the alloys. Consequently, the measured temperatures have dropped considerably below the calculated curves, as shown in Figures 8 and 9. Concerning other measurements [10,11] it is more difficult to explain the reason for the low temperature values of some points (see Figures 6 and 7).

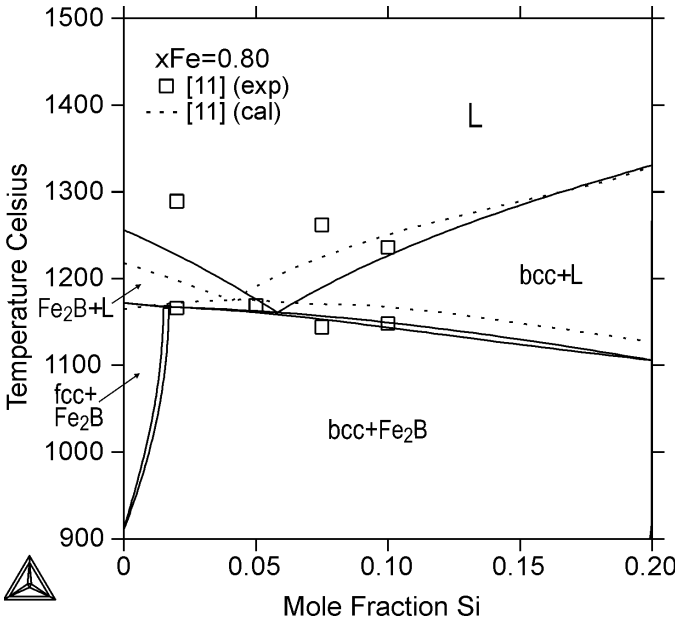

Fig. 6. Calculated vertical section at Fe molar fractionof $x_{Fe} = 0.80$ in the Fe-B-Si system, together with experimental data points of Poletti and Battezzati [11]. The solid curves refer to the calculations of this study and the dotted curves refer to those of Tokunga et al. [10] for the liquidus surface and the eutectic temperature line

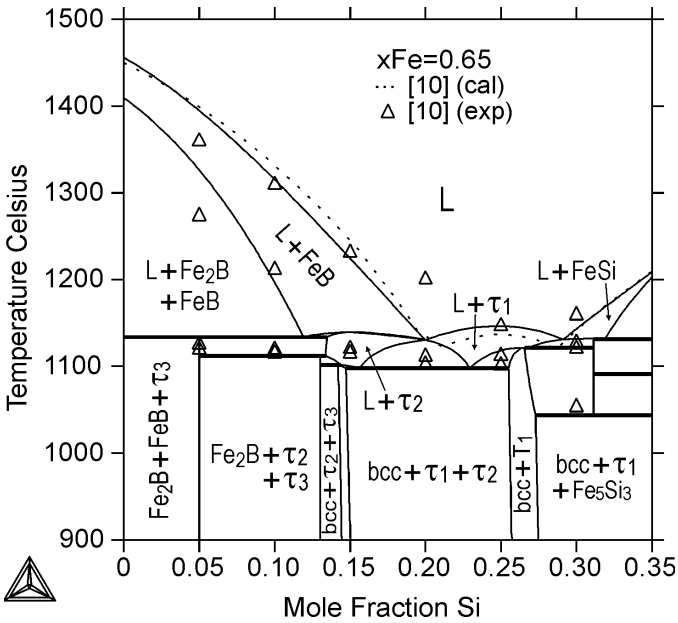

Fig. 7. Calculated vertical section at Fe molar fractionof $x_{Fe} = 0.65$ in the Fe-B-Si system, together with experimental data points of Tokunga et al. [10]. The solid curves refer to the calculations of this study and the dotted curves refer to those of [10] for the liquidus surface

Vertical sections at $x_{Fe} = 0.65$ (Fig. 7) and at $x_{Si} = 0.10$ (Figure 9) have also been calculated by Poletti and Battezzati [11].

Their results agree slightly better with the measurements than the current calculations, which is partly due to their different Fe-B system description.

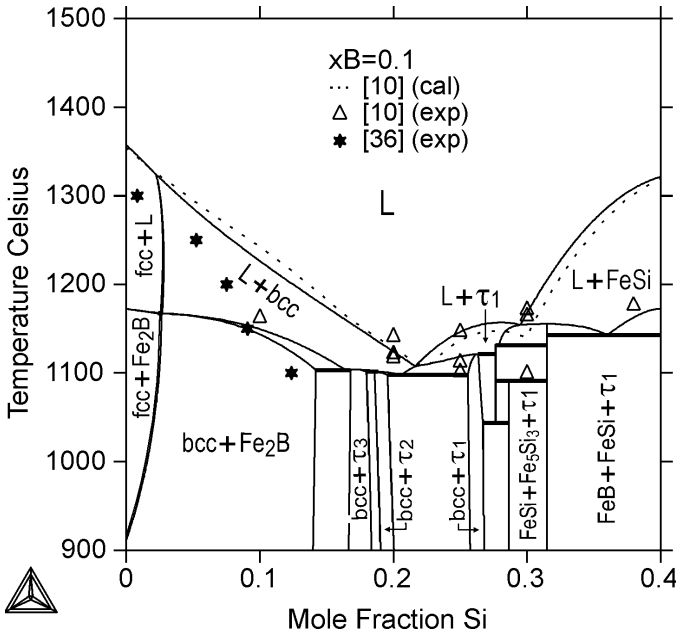

Fig. 8. Calculated vertical section at B molar fraction of $x_B = 0.10$ in the Fe-B-Si system, together with experimental data points of Tokunga et al. [10] and Nagumo and Sato [36]. Solid lines refer to the calculations of this study and dotted lines refer to those of [10] for the liquidus surface

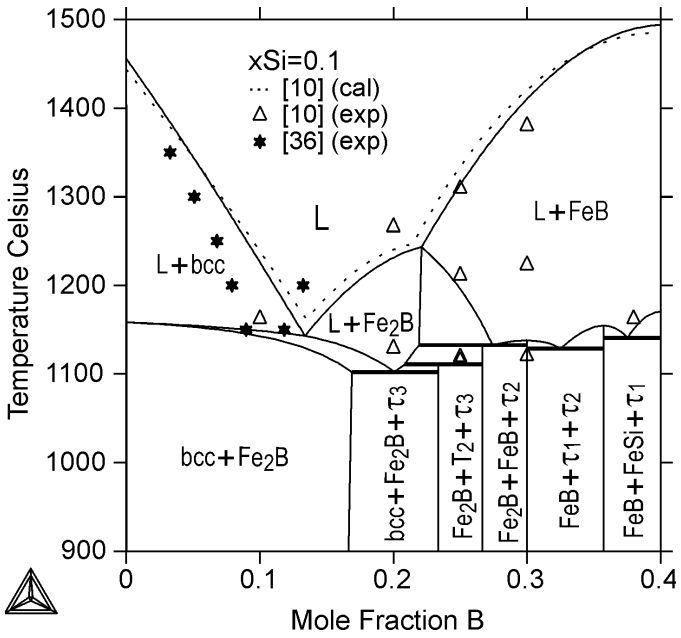

Fig. 9. Calculated vertical section at Si molar fraction of $x_{Si} = 0.10$ in the Fe-B-Si system, together with experimental data points of Tokunga et al. [10] and Nagumo and Sato [36]. Solid lines refer to the calculations of this study and dotted lines refer to those of [10] for the liquidus surface

Figures 10-15 demonstrate the calculated ternary liquid phase mixing enthalpy and Gibbs energy of formation (Figures 15 and 11) and the calculated partial molar Gibbs energies of Si and B in the ternary liquid phase (Figures 12-15). In every case, the agreement with the experimental data is good and slightly better than those calculated by [10,11].

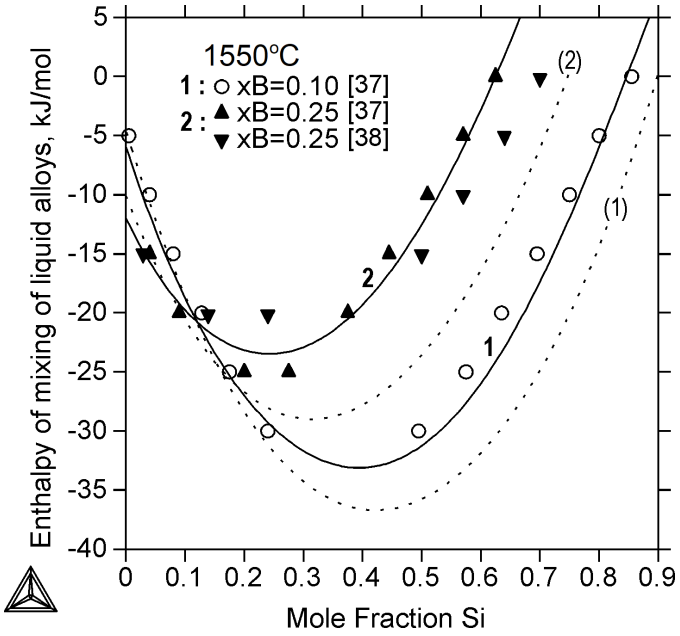

Fig. 10. Calculated integral molar enthalpy of mixing of liquid Fe-B-Si alloys at 1550°C, together with experimental data points of Zaitsev et al. [37] and Witusieviczet al. [38]. Solid lines refer to the current calculations and dotted lines show those of Poletti and Battezzati [11]. The reference states used are pure liquid Fe and Si and beta-rhombo B (pure solid B)

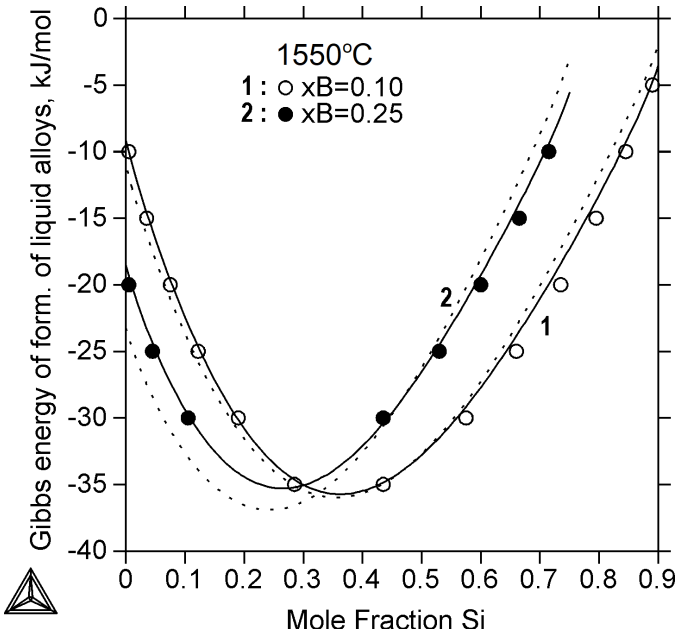

Fig. 11. Calculated integral molar Gibbs energy of formation of liquid Fe-B-Si alloys at 1550°C, together with experimental data points of Zaitsev et al. [37]. Solid lines refer to the current calculations and dotted lines show those of Poletti and Battezzati [11]. The reference states used are pure liquid Fe and Si and beta-rhombo B (pure solid B)

The calculated boron solubility in the *fcc* and *bcc* phases is shown in Figure 16. The Si content increase promotes the

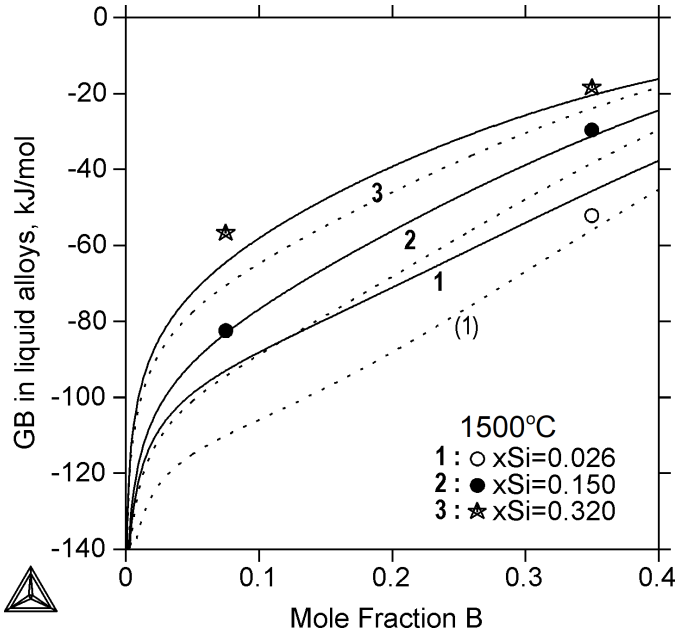

Fig. 12. Calculated chemical potential of B (GB, kJ/mol) in liquid Fe-B-Si alloys at 1500°C, together with experimental data points of Zaitsev et al. [37]. Solid lines refer to the current calculations and dotted lines show those of Poletti and Battezzati [11]. The reference state used is pure liquid B

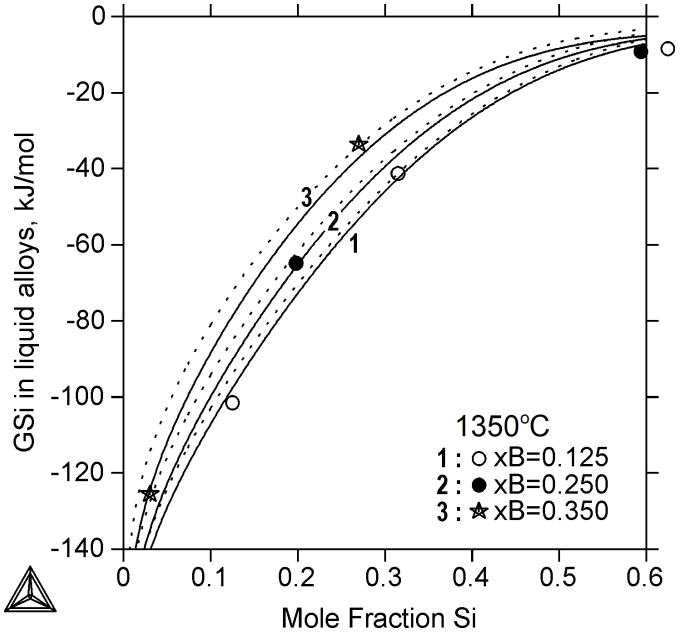

Fig. 14. Calculated chemical potential of Si (GSi, kJ/mol) in liquid Fe-B-Si alloys at 1350°C, together with experimental data points of Zaitsev et al. [37]. Solid lines refer to the current calculations and dotted lines show those of Poletti and Battezzati [11]. The reference state used is pure liquid Si

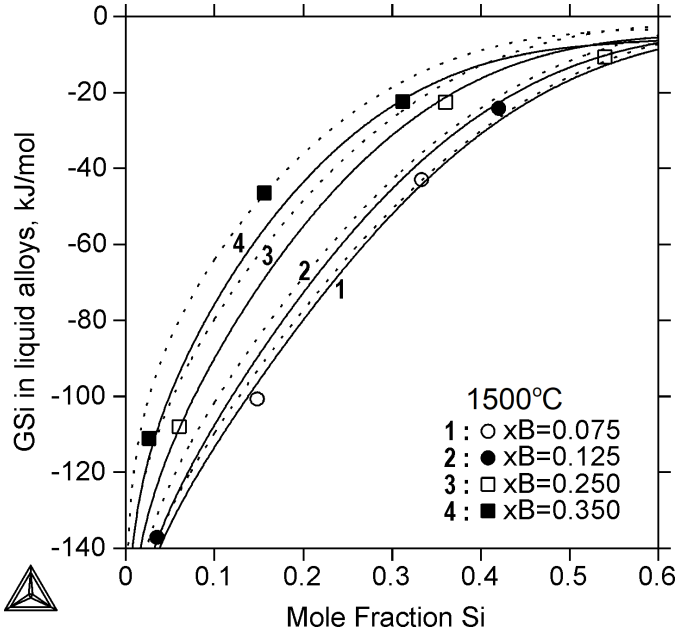

Fig. 13. Calculated chemical potential of Si (GSi, kJ/mol) in liquid Fe-B-Si alloys at 1500°C, together with experimental data points of Zaitsev et al. [37]. Solid lines refer to the current calculations and dotted lines show those of Poletti and Battezzati [11]. The reference state used is pure liquid Si

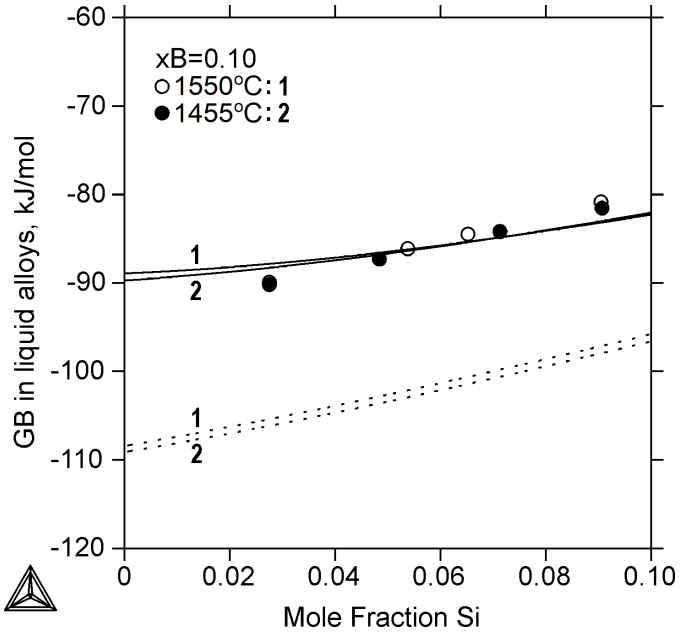

Fig. 15. Calculated chemical potential of B (GB, kJ/mol) in liquid Fe-B-Si alloys at B mole fraction of $x_B = 0.10$, together with experimental data points of Ball [39]. Solid lines refer to the current calculations and dotted lines show those of Poletti and Battezzati [11]. The reference state used is pure liquid B

formation of Fe_2B, which slightly decreases the boron solubility. The latter diminishes with the temperature decrease from 1150 to 1000°C as well. Additional experimental thermodynamic data about Si activity in liquid alloys are available from Ji et al. [45], but these are not consistent with the calculations and the experimental data of Zaitsev et al. [37].

5. Conclusions

This work represents a step toward extending the thermodynamic Iron Alloys Database to be used to simulate the non-equilibrium solidification and solid-state phase transformations of steels. The thermodynamic descriptions of the Fe-B and Fe-Si

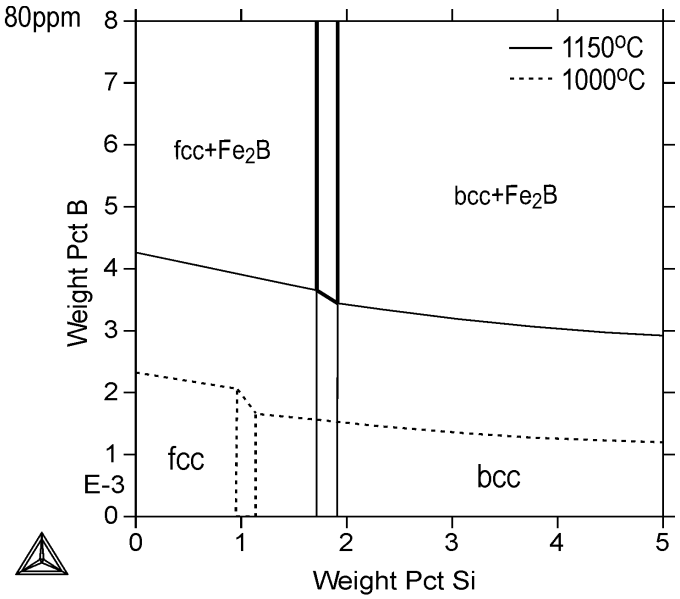

Fig. 16. Calculated B solubility in fcc and bcc phases of the Fe-B-Si system at 1150 and 1000°C

were retained from already published sources. The parameters of the other binary sub-system, B-Si, were reassessed. For the sake of consistency and simplicity of the whole database, B was permitted to form substitutional solutions in the B-Si and Fe-B-Si systems. In these descriptions, 18 phases, i.e., liquid, bcc, fcc,dia, beta-rhombo-B, Fe_2Si, Fe_5Si_3, FeSi, $FeSi_2$-H, $FeSi_2$-L, Fe_2B, FeB, SiB_n, SiB_6, SiB_3, $Fe_{47}Si_{20}B_{10}$, $Fe_{50}Si_{10}B_{20}$ and $Fe_{20}Si_4B_6$, have been considered. Experimental thermodynamic and topological data have been used for the optimization of the B-Si and Fe-B-Si systems. The calculated and experimental thermodynamic and phase equilibrium data were found to be in good agreement.

Acknowledgement

This study was executed within the framework of the Genome of Steel profiling project. The Academy of Finland (project 311934) and Walter Ahlström Foundation are acknowledged for funding this work.

REFERENCES

[1] J. Miettinen, G. Vassilev, Arch. Metall. Mater. **59**, 601 (2014).
[2] J. Miettinen, G. Vassilev, Arch. Metall. Mater. **59**, 609 (2014).
[3] J. Miettinen, K. Lilova, G. Vassilev, Arch. Metall. Mater. **59**, 1481 (2014).
[4] J. Miettinen, V-V. Visuri, T. Fabritius, N. Milcheva, G. Vassilev, Arch. Metall. Mater. **64**, 451 (2019).
[5] J. Miettinen, V.-V. Visuri, T. Fabritius, Acta Univ. Oul. **C704** (2019).
[6] J. Miettinen,S. Louhenkilpi, H. Kytönen, J. Laine, Math. Comput. Simulat. **80**, 1536 (2010).
[7] J. Miettinen, Metall. Mater. Trans. A **23A** 1155 (1992).
[8] J. Miettinen, S. Louhenkilpi, V.-V. Visuri,T. Fabritius, IOP Conf. Ser.: Mater. Sci. Eng. **529**, 012063 (2019).
[9] S. Louhenkilpi, J. Miettinen, J. Laine, R. Vesanen, I. Rentola, J. Moilanen, V.-V. Visuri, E.-P. Heikkinen, A. Jokilaakso, IOP Conf. Ser.: Mater. Sci. Eng. **529**, 012051 (2019).
[10] T. Tokunga, H. Ohtani , M. Hasebe, CALPHAD **28**, 354 (2004).
[11] M.G. Poletti, L. Battezzati, CALPHAD **43**, 40 (2013).
[12] J. Miettinen, G. Vassilev-Urumov, J. Phase Equil. Diff. **37**, 540 (2016).
[13] J. Lacaze, B. Sundman, Metall. Trans. A **22A**, 2211 (1991).
[14] J. Miettinen, CALPHAD **22**, 231 (1998).
[15] A.I. Zaitsev, A.A. Kodentsov, J. Phase Equilib. **22**, 126 (2001).
[16] A.T. Dinsdale, SGTE unary database, version 4.4; www.sgte.org.
[17] I. Ansara, A.T. Dinsdale, M.H. Rand, COST 507 – Thermochemical database for light metal alloys **Vol. 2**, European Communities, Belgium, (1998).
[18] S. Fries, H.L. Lukas, In: COST 507 – Thermochemical database for light metal alloys, **Vol. 2**, I. Ansara, A.T. Dinsdale, M.H. Rand eds., European Communities, Belgium, 126 (1998).
[19] T. Tokunga, K. Nishio, H. Ohtani, M. Hasebe, Mater. Trans. **44**, 1651 (2003).
[20] A. Dinsdale, A. Kroupa, A. Watson, J. Vrestal, A. Zemanova, P. Broz, COST action MP0602 -Handbook of High-Temperature lead-Free Solders - Atlas of Phase Diagrams, Vol. 1 ISBN 978-80-905363-1-9, Printed in the Czech Republic, 2012, pp 2018.
[21] O. Redlich, A.T. Kister, Ind. Eng. Chem. **10**, 345 (1948).
[22] Y.M. Muggianu, M. Gambino, P. Bros, J. Chim. Phys. **72**, 83 (1975).
[23] M. Hillert, M. Jarl, CALPHAD **2**, 227 (1978).
[24] B. Aronsson, I. Engström, Acta Chem. Scand. **14**, 1403 (1960).
[25] N.F. Chaban, Yu.B. Kuzma, Inorg. Mater. **6**, 883 (1970).
[26] Yu.V. Efimov, G.G. Mukhin, E.M. Lazarev, N.A. Korotkov, L.A. Ryabtsev, V.N. Dmitriev, T.M. Frolova, Russ. Metall. **4**, 167 (1986).
[27] V. Raghavan, Phase Diagrams of Ternary Iron Alloys – **Part 6A**, Indian Institute of Metals, Calcutta, 406 (1992).
[28] C. Brosset, B. Magnusson, Nature **187**, 54 (1960).
[29] G.V. Samsonov, V.M. Sleptsov, Dopovidi Akad. Nauk Ukr. RSR No.**8**, 1066 (1962).
[30] G.V. Samsonov, V.M. Sleptsov, J. Inorg. Chem. **8**, 2009 (1963).
[31] J. Hesse, Z. Metallkd. **59**, 499 (1968).
[32] B. Armas, G. Male, D. Salanoubat, C. Chatillon, M. Allibert, J. Less Com. Met., **82**, 245 (1981).
[33] G. Male, D. Salanoubat, Rev. Int. Hautes Temper. Refract. **18**, 109 (1981).
[34] R.W. Olesinski, G.J. Abbaschian, Bull. Alloy Phase Diagrams **5**, 478 (1984).
[35] P. Desre, I. Ansara, P. Cremer, J.C. Joud, CALPHAD **23**, 89 (1989).
[36] M. Nagumo, T. Sato, Suppl. Sci. Rep. RITU. **A**, 136 (1980).
[37] A.I. Zaitsev, N.E. Zaitseva, A.A. Kodentsov, Metall. Mater. Trans. B **34B**, 887 (2003).
[38] V.T. Witusievicz, A.A. Shcheretskii, A.K. Biletskii, V.S. Schumikhin, Rasplavy **4**, 102 (1989).
[39] D.L. Ball, Trans. Met. Soc. AIME **239**, 31 (1967).
[40] B. Hallemans, Wollants, J.R. Roos, Z. Metallkd. **85**, 676 (1994).

[41] J-O. Andersson, T. Helander, L. Höglund, P. Shi, B. Sundman, CALPHAD **26**, 273 (2002).

[42] R. Noguchi, K. Suzuki, F. Tsukihashi, N. Sano, Metall. Mater. Trans. B **25**, 903 (1994).

[43] G. Inoue, T. Yoshikawa, K. Morita, High Temp. Mat. Proc. **22**, 221 (2003).

[44] T. Yoshikawa, K. Morita, Mater. Trans. JIM **46**, 1335 (2005).

[45] C. Ji, R. Yu, S. Liu, Jinshu Xuebao **24**, B87 (1988).